Doping Asymmetry and Layer-Selective Metal-Insulator Transition in Trilayer $K_{3+x}C_{60}$

Changming Yue [ORCID],[1,*] Yusuke Nomura [ORCID],[2] and Philipp Werner [ORCID][1,†]

[1]*Department of Physics, University of Fribourg, 1700 Fribourg, Switzerland*
[2]*Department of Applied Physics and Physico-Informatics, Keio University, 3-14-1 Hiyoshi, Kohoku-ku, Yokohama 223-8522, Japan*

Thin films provide a versatile platform to tune electron correlations and explore new physics in strongly correlated materials. Epitaxially grown thin films of the alkali-doped fulleride $K_{3+x}C_{60}$, for example, exhibit intriguing phenomena, including Mott transitions and superconductivity, depending on dimensionality and doping. Surprisingly, in the trilayer case, a strong electron-hole doping asymmetry has been observed in the superconducting phase, which is absent in the three-dimensional bulk limit. Using density-functional theory plus dynamical mean-field theory, we show that this doping asymmetry results from a substantial charge reshuffling from the top layer to the middle layer. While the nominal filling per fullerene is close to $n = 3$, the top layer rapidly switches to an $n = 2$ insulating state upon hole doping, which implies a doping asymmetry of the superconducting gap. The interlayer charge transfer and layer-selective metal-insulator transition result from the interplay between crystal field splittings, strong Coulomb interactions, and an effectively negative Hund coupling. This peculiar charge reshuffling is absent in the monolayer system, which is an $n = 3$ Mott insulator, as expected from the nominal filling.

Introduction.—The alkali-doped fullerides A_3C_{60} (A = K, Rb, Cs) exhibit a remarkably high superconducting critical temperature in the range of 20–40 K, and several properties suggest an unconventional pairing mechanism [1–5]. The materials are strongly correlated three-orbital systems, with an intra-orbital interaction U comparable to the bandwidth W of about 0.5 eV [6]. Intriguingly, s-wave superconductivity, which had been believed to be fragile to strong electron correlations, appears in the vicinity of a Mott phase [1]. As U/W is tuned via chemical or physical pressure, a T_c dome is observed [7], and the metallic phase above this dome exhibits unusual properties on the strong-coupling side. More specifically, a Jahn-Teller metal with coexisting metallic and Mott insulating orbitals has been experimentally observed [7] and theoretically explained as a spontaneous orbital selective Mott phase [8]. The local singlet pairing and unusual normal-state properties of fulleride superconductors originate from the negative effective Hund coupling $J \approx -0.02$ eV, which results from the overscreening of the very small static Hund coupling $J_{\mathrm{Coulomb}} \approx 0.03$ eV in this molecular crystal by Jahn-Teller phonons [9], $\Delta J_{\mathrm{Jahn\text{-}Teller}} \approx -0.05$ eV. This produces an orbital-freezing in the strongly correlated metal regime, and the associated local orbital fluctuations have been suggested to play a key role in the pairing mechanism [8,10], in contrast to the spin freezing that is commonly associated with unconventional superconductivity in positive-J systems [11,12]. While many interesting properties and (doping-dependent) phase diagrams for A_3C_{60} type systems have been revealed by model and *ab initio*

calculations [2,3,8–10,13], experimental progress has been hampered by difficulties in preparing bulk single crystals.

Thin films offer a promising route to explore an expanded phase space of correlated materials. Many strongly correlated systems exhibit novel properties at interfaces or in the limit of few atomic layers. Prominent examples are correlated metallic or superconducting states at the interface between Mott and band insulators [14,15], or the remarkably high superconducting T_c in monolayer FeSe [16–22]. It is thus an interesting question what kind of correlation effects appear in fulleride compounds as one reduces the dimensionality from 3D to 2D.

Thin films of A_3C_{60} have been realized already more than 20 years ago [23,24], but the recent systematic study of the superconducting properties of epitaxially grown high-quality thin films of $K_{3+x}C_{60}$ represents an important step towards a detailed investigation of fulleride compounds [25]. These multilayer systems are single crystals, which allow us to study the effects of dimensionality (3D → 2D) and number of layers. Scanning tunneling microscopy (STM) can be used to obtain accurate information on the electronic states in the top layer [Fig. 1(e)]. Furthermore, by varying the concentration of the alkali atoms, these three-orbital systems can be doped over a wide range $n = 3 + x$ relative to the half-filled stoichiometric compound ($n = 3$). The STM results [25] demonstrated a Mott insulator to metal (or superconductor) transition with increasing number of layers, which may be explained by the larger screening and connectivity in the 3D limit. More surprisingly, in the superconducting trilayer samples, a very strong asymmetry in the gap size with respect to electron and hole doping was

observed. While hole doping quickly destroys the superconducting state, the latter is remarkably robust to electron doping. This is in stark contrast to 3D bulk systems [26], which do not show any significant doping asymmetry. Filling-dependent changes in the screening properties have been suggested as a possible mechanism [25], but this is unlikely to fully explain the observed strong asymmetry.

Here, using realistic simulations of trilayer $K_{3+x}C_{60}$ based on density functional theory (DFT) [27] and dynamical mean-field theory (DMFT) [28], we show that charge reshuffling between the layers and a layer-selective metal-insulator transition is at the origin of the doping asymmetry. In particular, even though the naively expected filling is close to $n = 3$, hole doping quickly leads to the formation of an $n = 2$ insulating state in the top layer, with one almost fully occupied and two almost empty orbitals, while electron doping results in three partially filled metallic orbitals.

Metal-insulator transitions in the negative-J model.—To set the stage, we first discuss the generic phase diagram of the negative-J three-orbital Hubbard model (Fig. 1), which assumes overscreening of J by phonons [4,5] (additional discussions on phonons can be found in the Supplemental Material [29], which includes Refs. [30–41]). In contrast to positive-J multiorbital systems, where the Hund coupling stabilizes the half-filled $n = 3$ Mott state, relative to the neighboring $n = 2$ and $n = 4$ Mott states [Fig. 1(a)], the effective $J < 0$ in $K_{3+x}C_{60}$ destabilizes the $n = 3$ Mott phase and pushes the critical on-site interaction to higher values [panel (b)]. In the absence of crystal-field splittings or asymmetries in the density of states (DOS), the $n = 2$ and $n = 4$ Mott states are equivalent (particle-hole symmetry), but in a layered system, a "two up, one down" splitting is introduced (see Table I), which favors the $n = 2$ insulating state with one almost completely filled and two almost empty orbitals [panel (c)]. This is a correlation-induced orbitally polarized insulator [42,43]. The insulating regions in Fig. 1 were obtained for a semicircular density of states, but realistic parameters and energy splittings.

The boundary of the s-wave superconducting phase is sketched in yellow based on the results reported in Ref. [13]. Considering the difference in dimensionality, one can imagine a situation where the half-filled ($n = 3$) monolayer is Mott insulating, and doping it does not result in a superconducting state (consistent with Ref. [44]), while the half-filled trilayer system is superconducting. In the trilayer case, because of the asymmetric situation, each layer can have a different filling and correlation strength. When a strongly correlated layer has a filling of $n < 3$, the existence of a very stable $n = 2$ insulating state may trigger a drastic charge reshuffling associated with a layer-selective metal-insulator transition. The realistic simulations below will show that this scenario is indeed realized in the top layer: the filling of the top layer of the $K_{3+x}C_{60}$ thin film is below half-filling already at $x = 0$ [see red star in panel (d)], and the top
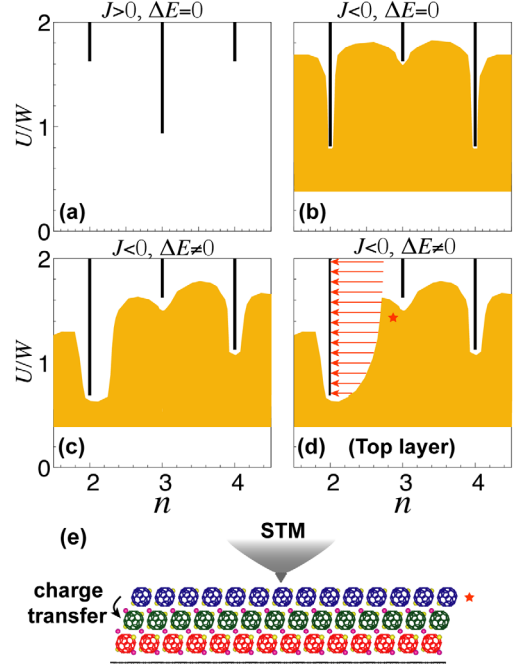

FIG. 1. Schematic phase diagram of three-orbital systems. (a) Generic phase diagram of an orbitally degenerate three-orbital Hubbard model with $J > 0$. The black lines indicate the Mott insulating solutions with filling $n = 2$, 3, and 4 and the white region a metallic solution. (b) Generic phase diagram of an orbitally degenerate three-orbital Hubbard model with $J < 0$. The yellow area shows the stability region of the s-wave superconducting phase at low temperatures. (c) Modification of the phase diagram by a crystal field splitting ΔE of the type two-up, one down, which favors the $n = 2$ insulating state. (d) Surface layer of the trilayer system. The red arrows indicate that there is no solution in the corresponding filling region, because of interlayer charge transfer which results in $n = 2$. The red star indicates the filling in the nominally undoped trilayer system. (e) STM measures the properties of the top layer.

layer quickly switches into an $n = 2$ insulating state upon hole doping $x < 0$ [red arrows in panel (d)] and charge transfer to the middle layer [black arrow in panel (e)].

Ab initio calculations.—Bulk K_3C_{60} has a face-centered cubic (fcc) structure, which can be viewed as close packing of (111) planes in a periodic sequence of $ABC\ ABC$ layers along the [111] direction, as shown in Fig. 2(a).

TABLE I. The effective level splittings $\Delta \tilde{E} = \tilde{E}_{2,3} - \tilde{E}_1$ of the trilayer $K_{3+x}C_{60}$ + substrate system for different dopings x at $T = 50$ K, $U = 0.7$ eV, and $J = -0.03$ eV. Here $\tilde{E}_i = E_i + \mathrm{Re}\Sigma_i^\infty$ is the effective energy level for the i-th orbital in a given layer. The numbers in parentheses are the bare crystal field splittings $\Delta E = E_{2,3} - E_1$. The energy unit is meV.

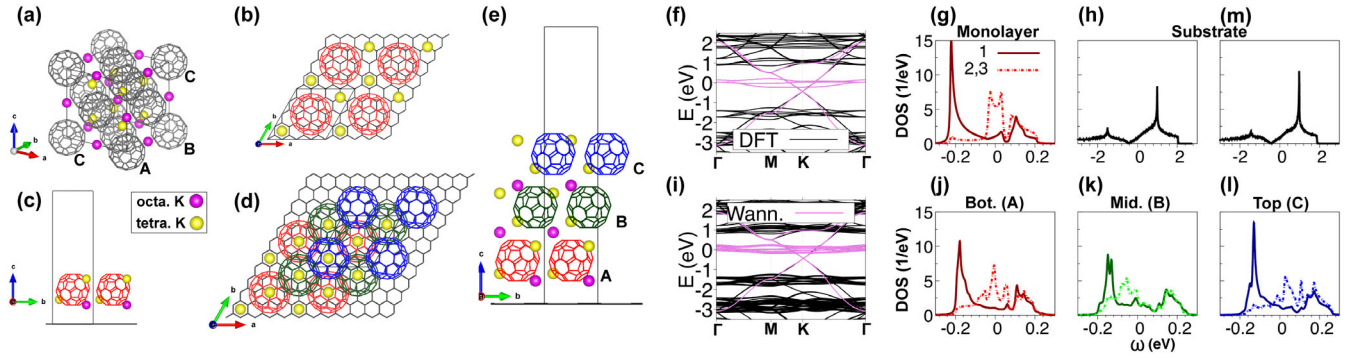| Doping x	Bottom layer (A)	Middle layer (B)	Top layer (C)
−0.1	679.2	114.5	908.1
0	681.6 (61.8)	230.0 (21.1)	696.9 (82.7)
0.1	677.7	113.5	691.0

FIG. 2. Crystal structure and electronic structure of monolayer and trilayer K_3C_{60} with graphene substrate. (a) Conventional unit cell of bulk K_3C_{60}. (b)–(c) [(d)–(e)] Top and side view of monolayer [trilayer] K_3C_{60} with graphene substrate (honeycomb lattice). For better visualization, the bottom (A), middle (B) and top layer (C) of C_{60} in (b)–(e) are colored red, dark green, and blue, respectively. The primitive unit cell is marked by the rhombus in (b) and (d). The DFT (black) bands and their Wannier interpolations (violet) are shown in panels (f) for the monolayer and in panel (i) for the trilayer, respectively. The corresponding orbital-resolved DOS per spin for each layer are shown in panels (g) and (j)–(l), where the solid line with dark color shows the projected DOS for the lowest-energy orbital and the dot-dashed line with lighter color that for the degenerate higher-energy orbitals. Panels (h) and (m) plot the total DOS for the substrate in (c) and (d), respectively.

The $K_{3+x}C_{60}$ films with small doping x also crystallize into an fcc structure [25]. Monolayer K_3C_{60} consists of only the A layer [panels (b), (c)], while the trilayer system is constructed by stacking the A, B, and C layers [panels (d), (e)]. To study the effect of the substrate, we place the films on top of a single layer of graphene. Details of the DFT calculations and structure relaxation are provided in the Supplemental Material [29]. The resulting DFT band structures are shown in Figs. 2(f) and 2(i). In the case of the monolayer (trilayer) + substrate system, there are 3 (9) narrow t_{1u} bands derived from C_{60} and three wide bands from the graphene substrate near the Fermi energy. The tight-binding Hamiltonian is obtained from the maximally localized Wannier functions constructed by wannier90 [45,46], and reproduces the DFT dispersion near the Fermi energy, see violet lines in panels (f) and (i).

We consider the orbitals which diagonalize the on-site Hamiltonian. For the trilayer system, the energy splittings between these orbitals are listed in Table I. The splittings are substantial in the case of the monolayer (118 meV) and the top layer of the trilayer system (82.7 meV). The corresponding orbital-resolved DOS is shown in Fig. 2(g) for the monolayer and in Figs. 2(j)–2(l) for the trilayer. On the other hand, the asymmetry in the total DOS is not sufficiently strong near the Fermi level that the DFT picture could not explain the experimentally observed doping asymmetry. We also show, in panels (h) and (m), the DOS of the substrate in the monolayer [(h)] and trilayer [(m)] system, which due to the strong dispersion of the bands is small near the Fermi energy.

The DFT + DMFT calculations are performed using maximally localized Wannier functions [47] without charge self-consistency. Each layer is mapped to a three-orbital Anderson impurity model embedded in a self-consistent electron bath [48,49]. The self-energy for each layer is assumed to be local and orbital-diagonal, and the DMFT impurity problems are solved with local density-density interactions ($H_{int} = \sum_\alpha U n_{\alpha\uparrow} n_{\alpha\downarrow} + \sum_{\sigma,\alpha>\gamma}[(U-2J)n_{\alpha\sigma}n_{\gamma\bar\sigma} + (U-3J)n_{\alpha\sigma}n_{\gamma\sigma}]$ with $n_{\alpha\sigma}$ the spin-density in orbital α) using continuous-time quantum Monte Carlo simulations in the hybridization expansion (CT-HYB) implementation [50,51]. We choose realistic parameters for the on-site interaction ($U = 0.7$ eV) and effective Hund coupling ($J = -0.03$ eV), consistent with a recent *ab initio* study [9] and constrained random phase approximation estimates [6,52], and present results for temperature $T = 50$ K. Additional simulation details, including the results for a rotationally invariant interaction and the double counting correction used to shift the weakly correlated substrate bands relative to the strongly correlated fulleride bands, are discussed in the Supplemental Material [29], where we also demonstrate that our main conclusions do not rely on a fine-tuning of parameters.

Results.—The filling $n^{A,B,C}$ in the different layers is plotted as a function of doping x in Fig. 3(a). The first noteworthy observation is that relative to the nominal value of $n = 3$ per layer, the top layer (C) is slightly hole doped ($n^C \approx 2.96$), and layer B slightly electron doped ($n^B \approx 3.04$), layer A undoped ($n^A \approx 3.00$), while there is little charge transfer from or to the substrate [black lines in panel (a); note the different scale]. There is hence a charge reshuffling from the top layer with the lowest connectivity to the middle layer with the highest connectivity already in the half-filled system. Upon hole doping, we observe a significant additional charge transfer from the top layer C to the middle layer B [Fig. 1(e)], and the switching of the top layer C into a state with filling $n^C \approx 2$. Besides a sheet of potassium atoms in the octahedral position, the presence of the substrate introduces an asymmetry between the bottom and the top layer. As a result of strong correlations,
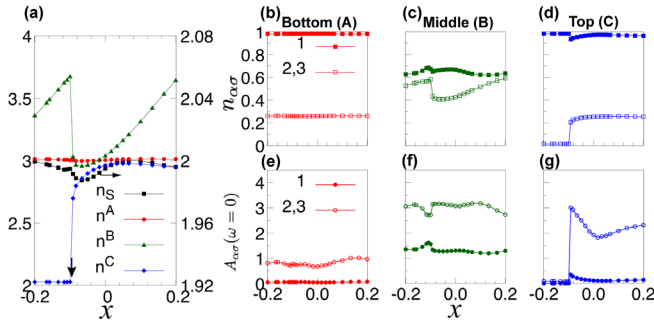
FIG. 3. DFT + DMFT results for the trilayer $K_{3+x}C_{60}$ + substrate system at $T = 50$ K, $U = 0.7$ eV, $J = -0.03$ eV. (a) Fillings in the different layers and in the substrate (S) as a function of doping x. (b)–(d) Orbital-resolved fillings per spin σ in the different layers as a function of x. (e)–(g) Orbital-resolved spectral weight per spin at $\omega = 0$ in the different layers as a function of x.
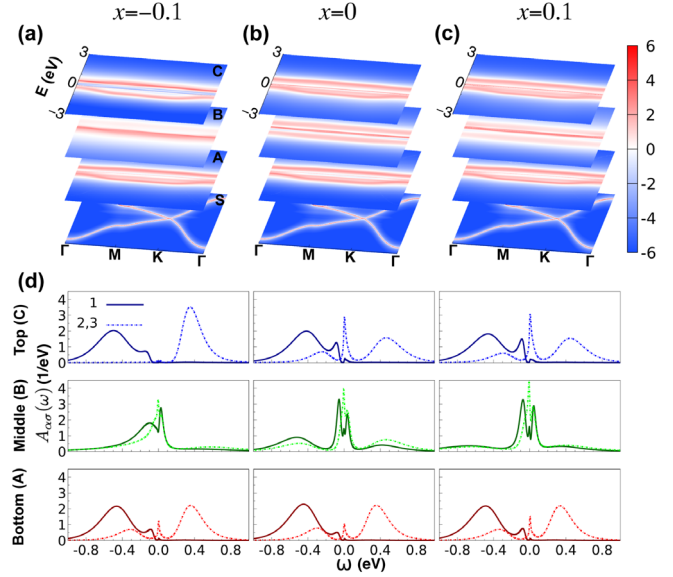

FIG. 4. DFT + DMFT spectra for the trilayer $K_{3+x}C_{60}$ + substrate system at $T = 50$ K, $U = 0.7$ eV, and $J = -0.03$ eV. (a)–(c) Momentum-resolved spectra $\log A(\mathbf{k}, \omega)$ for doping $x = -0.1$, 0, and 0.1. A, B, and C label the different layers and S the substrate. (d) Corresponding orbital-resolved local spectra per spin $A_{\alpha\sigma}(\omega)$. The thick lines correspond to orbital 1 and the dashed lines to orbitals 2, 3.

crystal field splittings, and this asymmetry, the trilayer system undergoes a layer-selective metal-insulator transition at small hole doping, while on the electron-doped side, a qualitatively different behavior with a stable metallic solution is found over a wide doping range.

More detailed information on the evolution of the doping in the different orbitals, as well as the spectral weight at the Fermi level, $A_{\alpha\sigma}(\omega = 0)$, is shown in panels (b)–(d) and (e)–(g), respectively. The results for layer A show that the occupation and low-energy spectral weight in this layer are only weakly dependent on doping x. The lower orbital 1 is essentially full and hence band insulating, while the two higher-lying orbitals 2, 3 are roughly quarter filled and metallic (see value of the spectral weight), but the almost vanishing charge compressibility indicates that they are on the verge of becoming Mott insulating. In the top layer C, all three orbitals undergo a metal-insulator transition around $x = -0.092$. Below this doping, the layer is in an orbitally polarized insulating state with an almost completely filled orbital 1 and almost empty orbitals 2 and 3. Above this doping, orbitals 2 and 3 are metallic with a filling and spectral weight that depends only weakly on x. As demonstrated in Ref. [53] (for a positive-J system), the transition from metal to orbitally polarized insulator depends sensitively on the details of the parameters U, J and the energy splitting $\Delta E = E_{2,3} - E_1$. In particular, the effective level splittings can be substantially enhanced by the real part of the self-energy $\Sigma_\alpha(\omega = \infty)$, which is also the case here, as one can see by comparing the effective level splittings $\Delta\tilde{E}$ (including the real part of the self-energy) in Table I to the bare splittings ΔE shown in brackets. The splittings in layers C and A are strongly enhanced, and the transition to the orbitally polarized insulator is associated with a further increase in the effective splitting in layer C. A qualitative difference to the previously discussed $J > 0$ model is that in the $J < 0$ system, the Hund coupling stabilizes the orbitally

polarized insulator, since the intra-orbital interaction is smaller than the interorbital one.

The orbitals in the most weakly correlated middle layer B remain metallic for all measured dopings x. By comparison between panels (c) and (d) we conclude that the metal-insulator transition in the top layer is associated with a transfer of charge to the higher-lying orbitals 2, 3 in the middle layer. Initially these orbitals absorb the holes, which results in an increasing orbital polarization with decreasing x, until the charge transfer from layer C associated with the metal-insulator transition reduces it substantially. Also upon electron doping, the extra charges are essentially absorbed by orbitals 2, 3 in the middle layer.

The layer-selective metal-insulator transition is also evident in the momentum-resolved spectral functions plotted in Fig. 4. Panel (b) shows the spectra of all layers and the substrate for the undoped system with $x = 0$, while panel (a) [(c)] shows the analogous results for a hole (electron) doped system with $x = -0.1$ ($x = 0.1$). The local spectra for the two types of orbitals are illustrated for layers A, B, and C in the corresponding subpanels of panel (d). The peaks near the Fermi level in the almost empty orbitals 2, 3 of the top layer result from hybridization with the partially filled orbital 1 [13,54].

Discussion and conclusions.—An orbitally polarized insulator will not become superconducting at even lower temperatures [25], while the metallic state in the considered parameter regime can be expected to do so [13]. Our finding of a strong doping asymmetry and metal-insulator transition

in the normal state thus provides a natural explanation for the experimentally observed asymmetry of the superconducting gap in the STM investigation of the trilayer structure. While the U value employed in this Letter (0.7 eV) is consistent with the *ab initio* study in Ref. [9], we have confirmed that our scenario for the asymmetry is robust with respect to a 10%–20% change in U (see Supplemental Material [29]). Also, the spectrum for the monolayer ($n = 3$ Mott insulator) is consistent with the STM spectrum [25]. The layer dependence of U may play some role in the different properties of the monolayer and trilayer systems, as discussed in Ref. [25], but our results suggest that the main difference arises from the interlayer hopping, which favors metallicity and enables the charge reshuffling associated with the layer-selective metal-insulator transition in the trilayer system.

In summary, the strong doping asymmetry observed in trilayer $K_{3+x}C_{60}$ is a consequence of correlation-enhanced crystal field splittings in few-layer thin films and the unusual properties of three-orbital systems with $J < 0$. The negative J stabilizes the $n = 2$ insulating state relative to the half-filled Mott state, so that hole doping in combination with interlayer charge transfer results in a metal-insulator transition in the surface layer for weak hole doping. The experimental results of Ref. [25] are thus a remarkable manifestation of the effectively inverted Hund coupling in fulleride compounds. Interesting open questions concern the effect of charge self-consistency, which, however, will be numerically very challenging for the trilayer system with 221 atoms per unit cell, the quantitative effect of the pair hopping term, which further enhances the interlayer charge transfer (see Supplemental Material [29]), and the study of the superconducting phase at even lower temperatures.

---

*changming.yue@unifr.ch
†philipp.werner@unifr.ch

[1] Y. Takabayashi and K. Prassides, Phil. Trans. R. Soc. A 374, 20150320 (2016).
[2] J. E. Han, O. Gunnarsson, and V. H. Crespi, Phys. Rev. Lett. 90, 167006 (2003).
[3] M. Capone, M. Fabrizio, C. Castellani, and E. Tosatti, Science 296, 2364 (2002).
[4] Massimo Capone, Michele Fabrizio, Claudio Castellani, and Erio Tosatti, Rev. Mod. Phys. 81, 943 (2009).
[5] Y. Nomura, S. Sakai, M. Capone, and R. Arita, J. Phys. Condens. Matter 28, 153001 (2016).
[6] Y. Nomura, K. Nakamura, and R. Arita, Phys. Rev. B 85, 155452 (2012).
[7] R. H. Zadik, Y. Takabayashi, G. Klupp et al., Sci. Adv. 1, e1500059 (2015).
[8] S. Hoshino and P. Werner, Phys. Rev. Lett. 118, 177002 (2017).
[9] Y. Nomura, S. Sakai, M. Capone, and R. Arita, Sci. Adv. 1, e1500568 (2015).
[10] C. Yue, S. Hoshino, A. Koga, and P. Werner, Phys. Rev. B 104, 075107 (2021).
[11] S. Hoshino and P. Werner, Phys. Rev. Lett. 115, 247001 (2015).
[12] P. Werner, S. Hoshino, and H. Shinaoka, Phys. Rev. B 94, 245134 (2016).
[13] C. Yue, S. Hoshino, and P. Werner, Phys. Rev. B 102, 195103 (2020).
[14] S. Okamoto and A. J. Millis, Nature (London) 428, 630 (2004).
[15] N. Reyren, S. Thiel, A. D. Caviglia et al., Science 317, 1196 (2007).
[16] Q.-Y. Wang, Z. Li, W.-H. Zhang et al., Chin. Phys. Lett. 29, 037402 (2012).
[17] D. Liu, W.-H. Zhang, D. Mou et al., Nat. Commun. 3, 931 (2012).
[18] S. He, J. He, W.-H. Zhang et al., Nat. Mater. 12, 605 (2013).
[19] S. Tan, Y. Zhang, M. Xia et al., Nat. Mater. 12, 634 (2013).
[20] Y. Zhang, J. J. Lee, R. G. Moore, W. Li, M. Yi, M. Hashimoto, D. H. Lu, T. P. Devereaux, D.-H. Lee, and Z.-X. Shen, Phys. Rev. Lett. 117, 117001 (2016).
[21] W.-H. Zhang, Y. Sun, J.-S. Zhang et al., Chin. Phys. Lett. 31, 017401 (2014).
[22] D. Huang and J. E. Hoffman, Annu. Rev. Condens. Matter Phys. 8, 311 (2017).
[23] S. Rogge, A. W. Dunn, T. Melin, C. Dekker, and L. J. Geerligs, Carbon 38, 1647 (2000).
[24] W. L. Yang, V. Brouet, X. J. Zhou et al., Science 300, 303 (2003).
[25] M.-Q. Ren, S. Han, S.-Z. Wang, J.-Q. Fan, C.-L. Song, X.-C. Ma, and Q.-K. Xue, Phys. Rev. Lett. 124, 187001 (2020).
[26] T. Yildirim, L. Barbedette, J. E. Fischer, C. L. Lin, J. Robert, P. Petit, and T. T. M. Palstra, Phys. Rev. Lett. 77, 167 (1996).
[27] W. Kohn and L. J. Sham, Phys. Rev. 140, A1133 (1965).
[28] A. Georges, G. Kotliar, W. Krauth, and M. J. Rozenberg, Rev. Mod. Phys. 68, 13 (1996).
[29] See Supplemental Material at http://link.aps.org/supplemental/10.1103/PhysRevLett.129.066403 details on methods, additional results for the monolayer + substrate systems and trilayer + substrate system, determination of substrate energy shift, effect of rotationally invariant interaction, and remarks on the Hubbard bands in STM and also on the effect of phonons.
[30] G. Kresse and J. Hafner, Phys. Rev. B 47, 558 (1993).

[31] G. Kresse and J. Furthmüller, Comput. Mater. Sci. **6**, 15 (1996).

[32] G. Kresse and J. Furthmüller, Phys. Rev. B **54**, 11169 (1996).

[33] H. Hafermann, K. R. Patton, and P. Werner, Phys. Rev. B **85**, 205106 (2012).

[34] Z. Zhong, M. Wallerberger, J. M. Tomczak, C. Taranto, N. Parragh, A. Toschi, G. Sangiovanni, and K. Held, Phys. Rev. Lett. **114**, 246401 (2015).

[35] X.-J. Han, P. Werner, and C. Honerkamp, Phys. Rev. B **103**, 125130 (2021).

[36] H. T. Dang, A. J. Millis, and Chris A. Marianetti, Phys. Rev. B **89**, 161113(R) (2014).

[37] O. Gunnarsson, Rev. Mod. Phys. **69**, 575 (1997).

[38] K. Steiner, Y. Nomura, and P. Werner, Phys. Rev. B **92**, 115123 (2015).

[39] Y. Nomura, M. Kaltak, K. Nakamura, C. Taranto, S. Sakai, A. Toschi, R. Arita, K. Held, G. Kresse, and M. Imada, Phys. Rev. B **86**, 085117 (2012).

[40] J. Kaufmann, P. Gunacker, A. Kowalski, G. Sangiovanni, and K. Held, Phys. Rev. B **100**, 075119 (2019).

[41] V. I. Anisimov, I. V. Solovyev, M. A. Korotin, M. T. Czyżyk, and G. A. Sawatzky, Phys. Rev. B **48**, 16929 (1993).

[42] M. Fabrizio and E. Tosatti, Phys. Rev. B **55**, 13465 (1997).

[43] M. Capone, M. Fabrizio, P. Giannozzi, and E. Tosatti, Phys. Rev. B **62**, 7619 (2000).

[44] J. Wu, Physica (Amsterdam) **439C**, 101 (2006).

[45] A. A. Mostofi, J. R. Yates, G. Pizzi, Y.-S. Lee, I. Souz, D. Vanderbilt, and N. Marzari, Comput. Phys. Commun. **185**, 2309 (2014).

[46] G. Pizzi, V. Vitale, R. Arita *et al.*, J. Phys. Condens. Matter **32**, 165902 (2020).

[47] F. Lechermann, A. Georges, A. Poteryaev, S. Biermann, M. Posternak, A. Yamasaki, and O. K. Andersen, Phys. Rev. B **74**, 125120 (2006).

[48] M. Potthoff and W. Nolting, Phys. Rev. B **60**, 7834 (1999).

[49] S. Sen, J. Moreno, M. Jarrell, and N. S. Vidhyadhiraja, Phys. Rev. B **91**, 155146 (2015).

[50] P. Werner, A. Comanac, L. de Medici, M. Troyer, and A. J. Millis, Phys. Rev. Lett. **97**, 076405 (2006).

[51] E. Gull, A. J. Millis, A. I. Lichtenstein, A. N. Rubtsov, M. Troyer, and P. Werner, Rev. Mod. Phys. **83**, 349 (2011).

[52] Y. Nomura and R. Arita, Phys. Rev. B **92**, 245108 (2015).

[53] P. Werner and A. J. Millis, Phys. Rev. Lett. **99**, 126405 (2007).

[54] R. Zitzler, Th. Pruschke, and R. Bulla, Eur. Phys. J. B **27**, 473 (2002).

[55] L. Huang, Y. Wang, Z. Y. Meng, L. Du, P. Werner, and X. Dai, Comput. Phys. Commun. **195**, 140 (2015).

[56] L. Huang, Comput. Phys. Commun. **221**, 423 (2017).